Global Journal of Science Frontier Research: H
Environment & Earth Science
Volume 16 Issue 5 Version 1.0 Year 2016
Type : Double Blind Peer Reviewed International Research Journal
Publisher: Global Journals Inc. (USA)
Online ISSN: 2249-4626 & Print ISSN: 0975-5896

The use of Airborne Spectrometric Data in Geological Mapping and Uranium Exploration at Qena-Quseir Shear Zone Area, Eastern Desert, Egypt

By Elkhadragy A. A., Ali M. S. Abdelaziz, Abdelmohsen G. N. Gharieb & Ahmed A. El-Husseiny
Zagazig University

Abstract- Qena-Quseir shear zone area is located at the central part of the Eastern Desert covering area of about 9460 Km^2. This area is mainly covered by basement rocks however there are parts covered by sedimentary rocks ranging in age from Upper Cretaceous to Quaternary. In this research, airborne gamma-ray spectrometric data is used to refinement of the mapped surface geology depending on the radioelements content between lithological assemblages. The gamma-ray data is also used for studying the distribution of the radioactive elements and determination of anomalous zones of uranium. The data were collected by Aeroservice department, Western geophysical company of America along flight lines oriented in a NE-SW direction with 1.5 Km line spacing and along tie lines oriented in NW-SE direction with 10 Km line spacing. Radioelements maps shows three levels of concentrations. The high level is related to younger granite, Duwi formation and some parts of Dokhan volcanics whereas the lowest level is related to metavolcanics.

GJSFR-H Classification: *FOR Code: 040399*

Strictly as per the compliance and regulations of :

The use of Airborne Spectrometric Data in Geological Mapping and Uranium Exploration at Qena-Quseir Shear Zone Area, Eastern Desert, Egypt

Elkhadragy A. A. [α], Ali M. S. Abdelaziz [σ], Abdelmohsen G. N. Gharieb [ρ] & Ahmed A. El-Husseiny [ω]

Abstract- Qena-Quseir shear zone area is located at the central part of the Eastern Desert covering area of about 9460 Km^2. This area is mainly covered by basement rocks however there are parts covered by sedimentary rocks ranging in age from Upper Cretaceous to Quaternary. In this research, airborne gamma-ray spectrometric data is used to refinement of the mapped surface geology depending on the radioelements content between lithological assemblages. The gamma-ray data is also used for studying the distribution of the radioactive elements and determination of anomalous zones of uranium. The data were collected by Aeroservice department, Western geophysical company of America along flight lines oriented in a NE-SW direction with 1.5 Km line spacing and along tie lines oriented in NW-SE direction with 10 Km line spacing. Radioelements maps shows three levels of concentrations. The high level is related to younger granite, Duwi formation and some parts of Dokhan volcanics whereas the lowest level is related to metavolcanics. Radioelements ratio map shows that the high level is compatible with Duwi formation, Younger granite and some parts of Dokhan volcanics. The radioelement composite image map display that the light zones is correlated with younger granite, Duwi formation and parts of Dokhan volcanics. Normality and Chi-Square ($\chi 2$) tests were applied to construct the interpreted radiometric lithologic unit (IRLU) map depending on the total count radiometric survey data. After applying normality and Chi-Square ($\chi 2$) tests, it is found that twenty-five rock units have normal distribution and eight rock units don't have. The rock units which is found to obey non-normal distribution are divided into two subunits. In this study, significant locations of eU anomalies are defined on the basis of calculation of probabilities, where their data differ significantly from the mean background, as defined by the data themselves, and at certain levels of probabilities these differences were computed. The high anomalous values are considered as the values equalling or exceeding at least two standard deviations from the calculated arithmetic mean values (X+2S) for eU, eU/eTh and eU/K measurements, for a single point in each rock unit. Fifteen groups of statistically significant (anomalous) points can be distinguished on urnium point anomaly map. Anomalies are concentrated in areas covered by Duwi formation, Younger granite and some parts of Dokhan volcanics.

Author α: Geology Departement, Faculty of Science, Zagazig University
Author σ ρ ω: Airborne Geophysics Department, Nuclear Materials Authority. e-mail: ahmednoureldin85@yahoo.com

I. Introduction

The area of study (Fig.1) is located at the central part of the Eastern Desert of Egypt (covering an area of 9460 Km^2). This area is mainly covered by basement rocks however there are parts covered by sedimentary rocks ranging in age from Upper Cretaceous to Quaternary.

Gamma-ray spectrometry usually used as one of good tools in geological mapping especially in areas of high terrain complex. The conventional approach to the acquisition and processing of airborne gamma-ray spectrometric data is to monitor three relatively broad spectral windows. These three elements named as potassium (K), equivalent uranium (eU) and equivalent thorium (eTh) windows have energy of 1.46 MeV, 1.76 MeV and 2.62 MeV respectively (IAEA, 2003). They are used for the measurement of K, U and Th.

The present study deals essentially with the analysis and interpretation of aerial spectral radiometric and magnetic survey data acquired over the study area. The data interpretation would be supplemented by the consideration of all available previous geological, geochemical and geophysical information in this area. In brief, the proposed study has two main objectives; the refinement of the mapped surface geology and determination of uranium anomalous zones.

II. Geological Background

Based on the geologic map of Egypt (Elramly, 1972), Stern and Hedge, 1985, identified three distinct basement domains in the Eastern Desert; these are the North, Central, and South Eastern Deserts. These areas were divided by two fault zones, and are abbreviated NED, CED, and SED. The present study area located at the transfer zone between NED and CED (Qena-Quseir shear zone). There is a much higher concentration of granitic rocks in the NED and SED than in the CED. The CED exposes, by far, the greatest concentration of rocks with strong oceanic affinities, such as ophiolites and Banded Iron Formation (BIF) (Sultan et al., 1988). The area is covered at the western side by sedimentary rocks ranging in age from upper Cretaceous to Quaternary (Fig. 2).

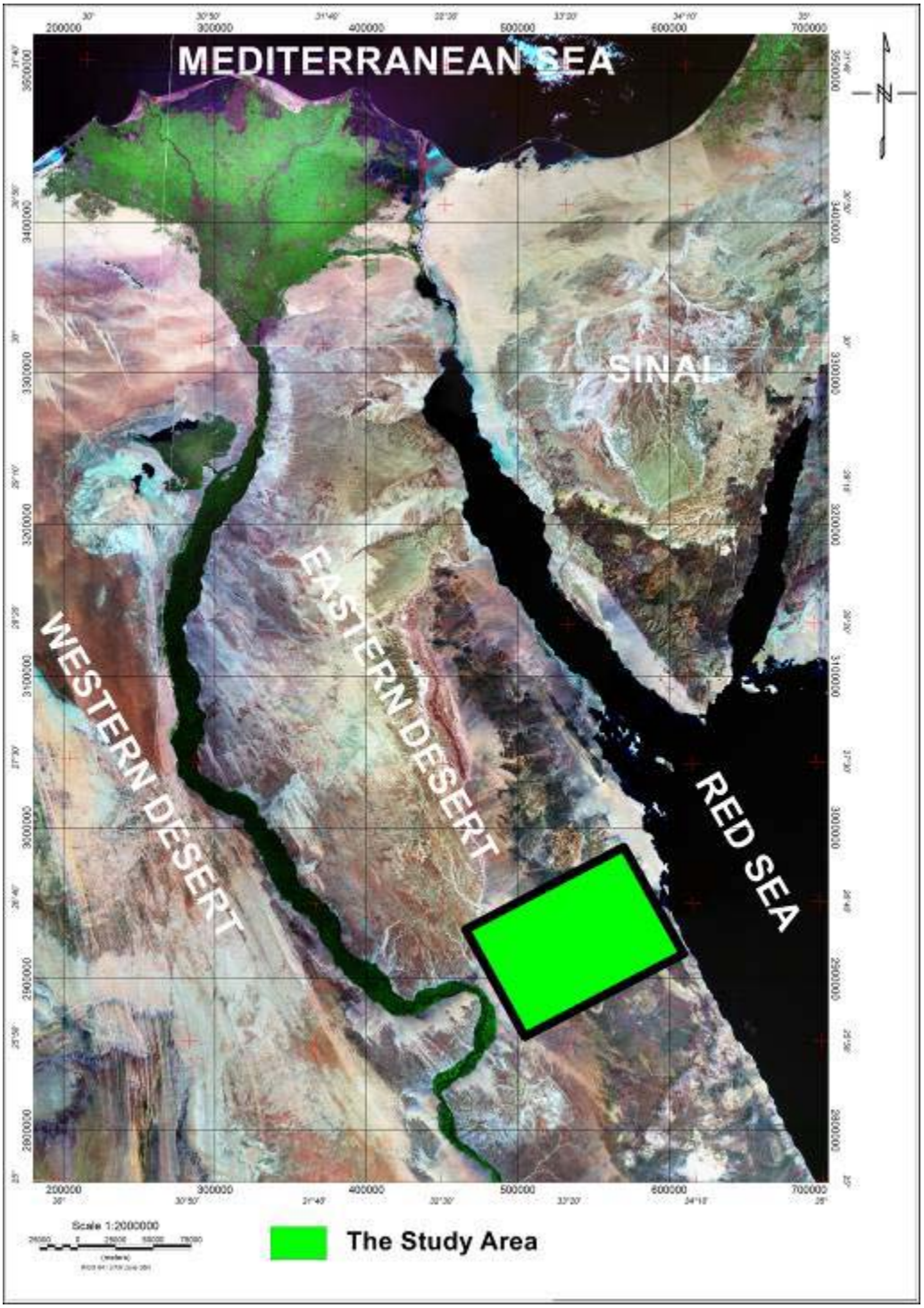

Figure (1): Satellite image showing location of the present study area

The rock units exposed in the study area could be arranged into four main groups; from older to younger units (Schandelmeier et al., 1983 & 1987; Greiling et al., 1988):

1- Pre-Pan-African rocks (gneisses and migmatites).
2- Pan-African ophiolites and island-arc assemblage (serpentinites, metagabbros, metavolcanics and metavolcaniclastics).
3- Cordilleran-stage associations (different types of granites).
4- Quaternary sediments.

The Eastern Desert of Egypt lies within the fold and thrust belt of the Pan-African continental margin orogeny (El- Gaby, 1983). It consists of relatively thin and imprecated thrust sheets overlying an attenuated Early Proterozoic continental margin.

Greiling, 1988 believe that the Pan African belt was created by compression from an easterly direction, while Shackleton et al. 1980, Ries et al. 1983, and Habeib et al. 1985) consider that the direction of tectonic transport was towards the NNW.

According to the constructed structural map (Conoco and EGPC, 1987), the fracture lineaments including faults have four main trend sets; NW - SE, NE – SW, ENE – WSW and E-W.

In the interior of the African–Nubian Shield, steep vertical movements are accepted and for the Precambrian rocks and the Phanerozoic rocks. These faults are often regenerated with quite steep graben borders intersecting the uplift in the Miocene age, in connection with the variations and oscillations in the vertical pattern of faulted areas on the plunges of old massifs, (Schurmann, 1974).

The orientation of the Late Paleozoic to Mesozoic large-scale undulations indicates that the reason for the SE–NW compression in the rotation tendency of Africa start in Carboniferous and culminate in Tertiary regions of Africa separated from Asia (Schurmann, 1974).

Being of epi-Hercynian age, they are generally filled with Triassic and Jurassic series. They are often thick, containing such volcanics such as andesite, basalt, and related tuff. Unlike the aulacogens of ancient platforms, scientists have suggested calling these depressions taphrogenes. The second stage in the young platforms is characterized by the generation of gentle uplifts, similar to shields, and by extensive and long-developing depressions looking like synclines and pericratonic down-warps of ancient platforms. The depressions were initiated in the Jurassic time and then developed during the Cretaceous, Paleogene, and Neogene times; some of them are subsiding at present.

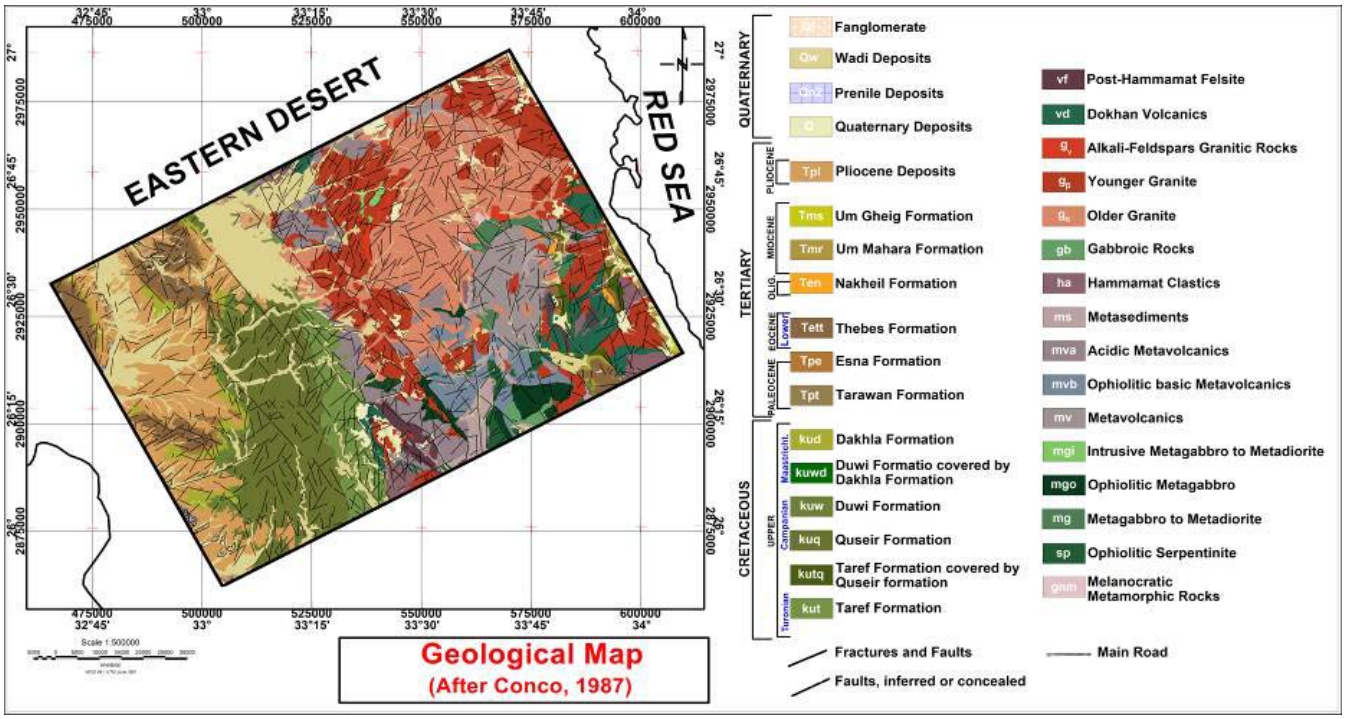

Figure (2): Geologic Map of Qena-Quseir Shear Zone Area, Central Eastern Desert, Egypt, (After Conco, 1987)

III. Aerospectrometric Data

In 17th December, 1984, Aero-Service Division, Western Geophysical Company of America conducted spectral gamma-ray survey covering an area of 9460 km^2 over Qena-Quseir shear zone area, Central Eastern Desert, Egypt (Fig. 1). The data were acquired along flight-lines oriented in NE-SW direction using 1.5 Km line spacing and along tie-lines oriented in NW-SE direction using 10000 m line spacing. Nominal flying elevation was 120m above ground surface (Aeroservice Report, 1984) (Fig. 3).

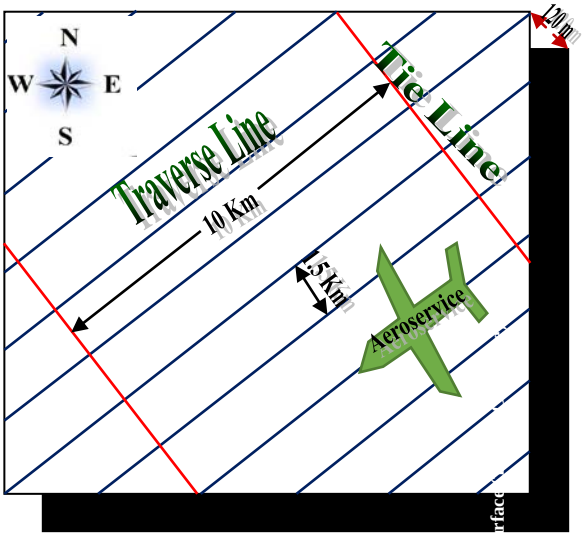

Figure (3): Flight Path Specifications of the Study Area (After Aeroservice, 1984)

The Aero-Service aircraft, registration number N80DS, twin-engine Cessna-Titan, type 404 was used for the data acquisition. A 35 mm path-recovery camera was used to record the ground track of the aircraft. High-sensitivity 256-channel (12 keV/channel) gamma-ray spectrometer system was used in measurement. The detectors system comprises primary (downward-looking) detector for measuring the terrestrial gamma radiation and secondary (or upward-looking) detector for measuring the atmospheric radon. The primary detector include three detector packages, each package consists of four crystals of high-resolution sodium iodide, thallium-activated (NaI "Tl") detectors of individual dimension 4x4x16 inches (256 cubic inches = 4195.088 cc = 4.195 litres). The four crystals in each package were put in intimate contact of dimension 16x16x4 inches (1024 cubic inches = 16780.35 cc = 16.78 litres). The total volume of the primary detector is 3072 cubic inches (50341.06 cc = 50.341 litres). The secondary or the upper-looking detector consists of two crystals of sodium iodide thallium-activated (NaI "Tl") detectors of the same dimension. The total volume of the secondary detector is 512 cubic inches (8390.176 cc = 8.39 litres). Each detection package is enclosed in a heated and thermally stabilized container to assure system spectral stability (Aero-Service Report, 1984).

A variety of analogue outputs from the data acquisition system (CODAS) developed by Aero-Service, 1984, may be software-selected by the system operator. For this type of survey, normal outputs were, total count (0.6-3.0 MeV), potassium (^{40}K) (1.37-1.57 MeV), uranium (^{214}Bi) (1.67-1.87 MeV), thorium (^{208}Tl) (2.41-2.82 MeV), and radar altimeter (100 feet/inch, i.e., 12 m/cm).

IV. Interpretation

a) Radioelements Maps Descriptions

The investigation of the four radioelements maps (TC, K, eU, eTh) (Figs. 4, 5, 6&7) shows that, these maps reflect three levels of radiometric concentrations. The first low radiometric level is less than 5 μR/h for total count, less than 0.4 % for potassium, less than 1.4 ppm for equivalent uranium and less than 2.4 ppm for equivalent thorium. This level is well compatible with metavolcanics, metagabbro and small parts of metasediments.

The second intermediate radiometric concentration level ranges from 5 to 11 μR/h for total count, from 0.4 to 1.4 % for potassium, from 1.4 to 2.7 ppm for equivalent uranium and from 2.4 to 5.5 ppm for equivalent thorium. This level is related to the sedimentary cover at the western part of the study area, some parts of older granite and small spots of metavolcanics.

The third high radiometric concentration level ranges from 11 to more than 25 μR/h for total count, from 1.4 to more than 3 % for potassium, from 2.7 to more than 8 ppm for equivalent uranium and from 5.5 to more than 15 ppm for equivalent thorium. This level is well-matched with younger granite, Duwi formation, parts of Dokhan volcanics and dispersed spots of older granite.

Careful examination of eU/eTh and eU/K ratio maps (Figs. 8&9) shows that, the distribution of eU/eTh and eU/K values are variable and spread over most geologic units, in the form of dispersed anomalies scattered in intermediate eU/eTh and eU/K background. The lowest values (less than 0.35 for eU/eTh and less than 1.2 for eU/K) are related to metavolcanics, metasediments and parts of younger granite. Meanwhile the highest values (more than 2.2 for eU/eTh and more than 17 for eU/K) are compatible with Duwi formation, Thebes formation, Dakhla formation and small parts of younger granite. Increasing of eU/eTh and eU/K values over the sedimentary rocks may be related to the uranium leaching process since it is mobile and leachable.

Different rock types have different characteristic concentrations of radioelements, potassium, uranium and thorium. Therefore, concentrations calculated from gamma -ray spectrometric data can be used to identify zones of consistent lithology and contacts between constraining lithologies (Duval, 1983).

It was noticed that, the highest light zones are clearly correlated with younger granitic rocks and some parts of Dokhan volcanics. Meanwhile, the poorly eU, eTh and K concentrations (black area in Fig. 10) covers metavolcanics, metasediments and metagabbro.

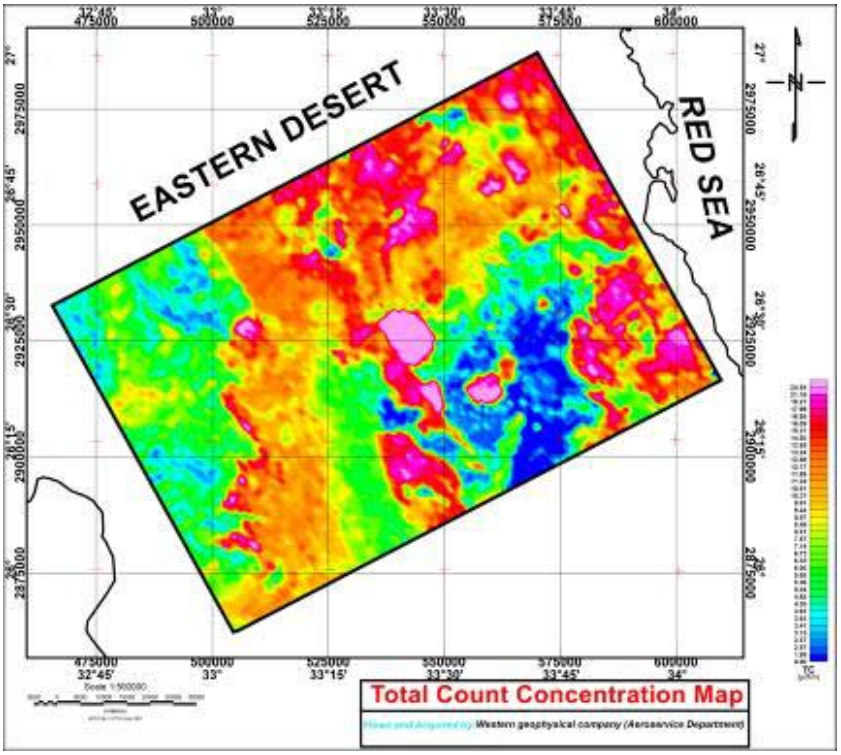

Figure (4): Filled Colour Contour Map of the Total Count Radiometric Data of Qena-Quseir Shear Zone area, Central Eastern Desert, Egypt

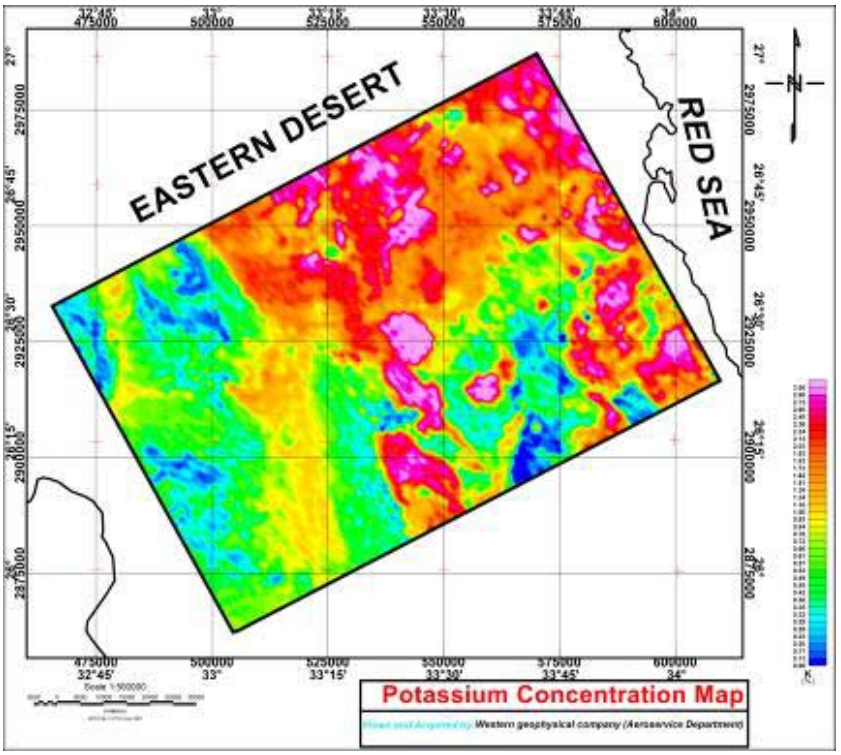

Figure (5): Filled Colour Contour Map of the Potassium Concentration of Qena-Quseir Shear Zone area, Central Eastern Desert, Egypt

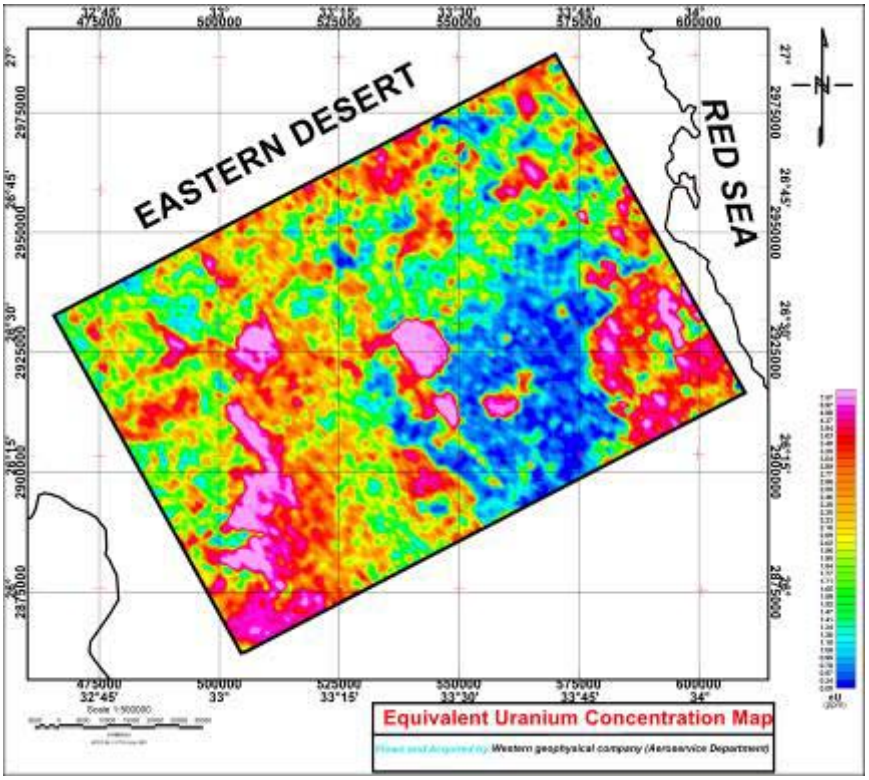

Figure (6): Filled Colour Contour Map of the Equivalent Uranium Concentration of Qena-Quseir Shear Zone area, Central Eastern Desert, Egypt.

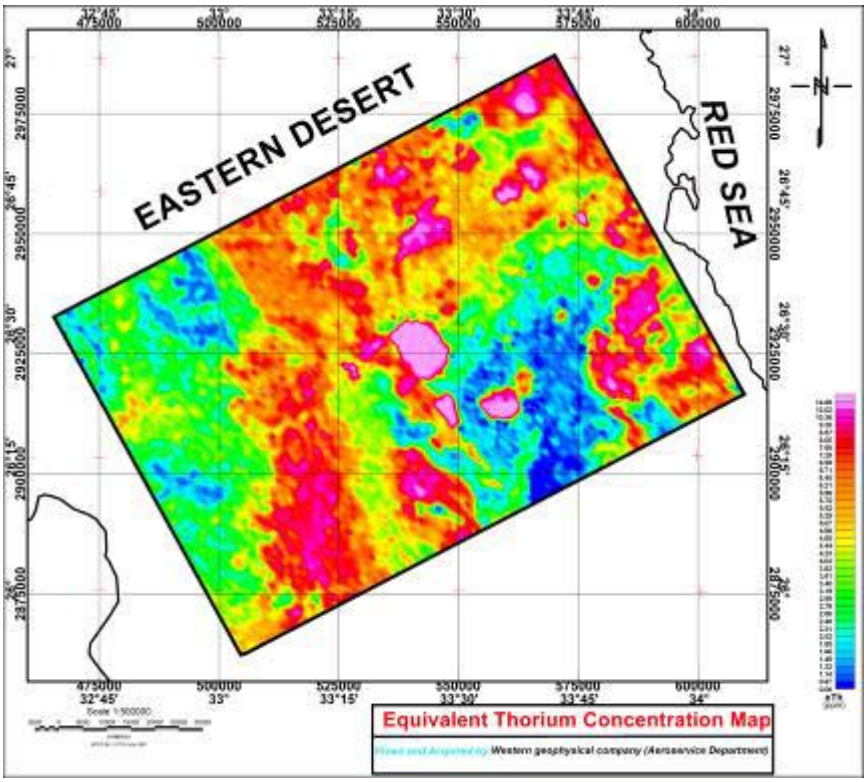

Figure (7): Filled Colour Contour Map of the Equivalent Thorium Concentration of Qena-Quseir Shear Zone area, Central Eastern Desert, Egypt.

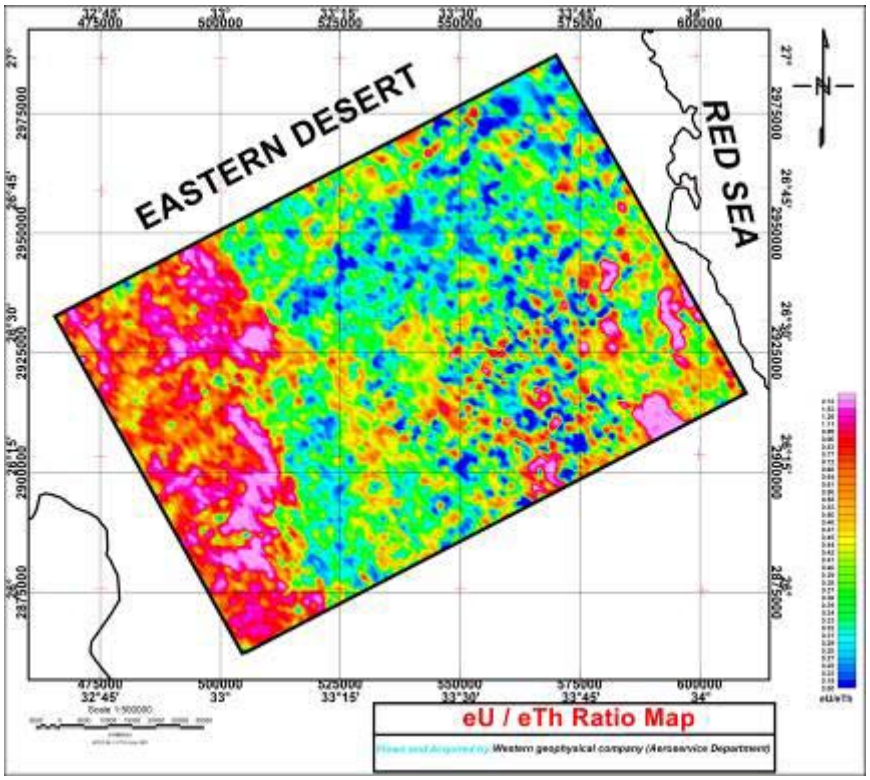

Figure (8): Filled Colour Contour Map of the Two-Radioelements (eU/eTh) Ratio of Qena-Quseir Shear Zone area, Central Eastern Desert, Egypt.

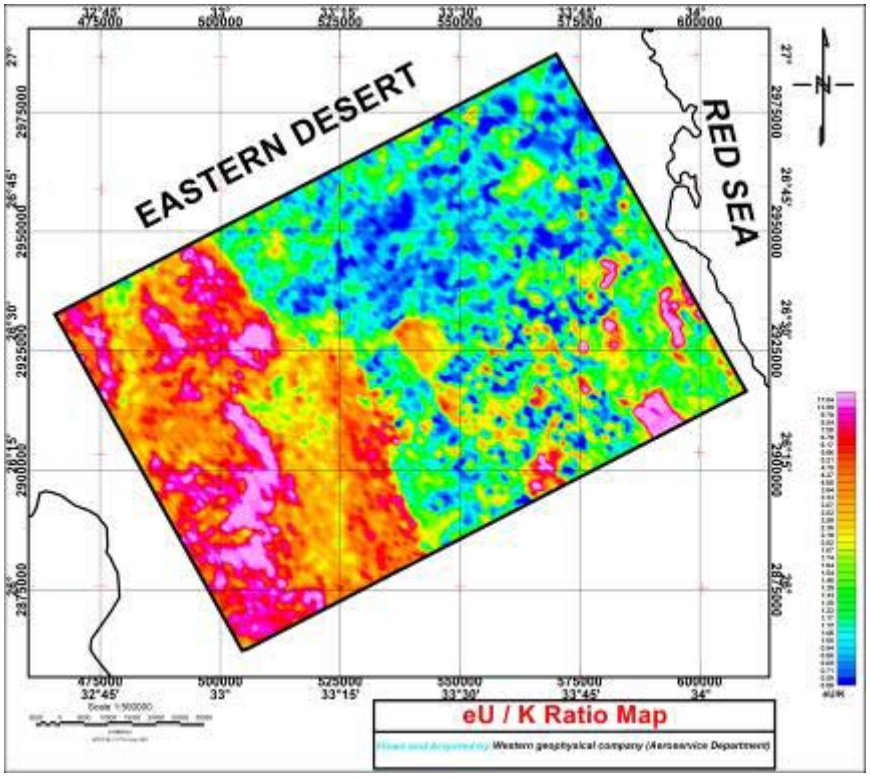

Figure (9): Filled Colour Contour Map of the Two-Radioelements (eU/eTh) Ratio of Qena-Quseir Shear Zone area, Central Eastern Desert, Egypt

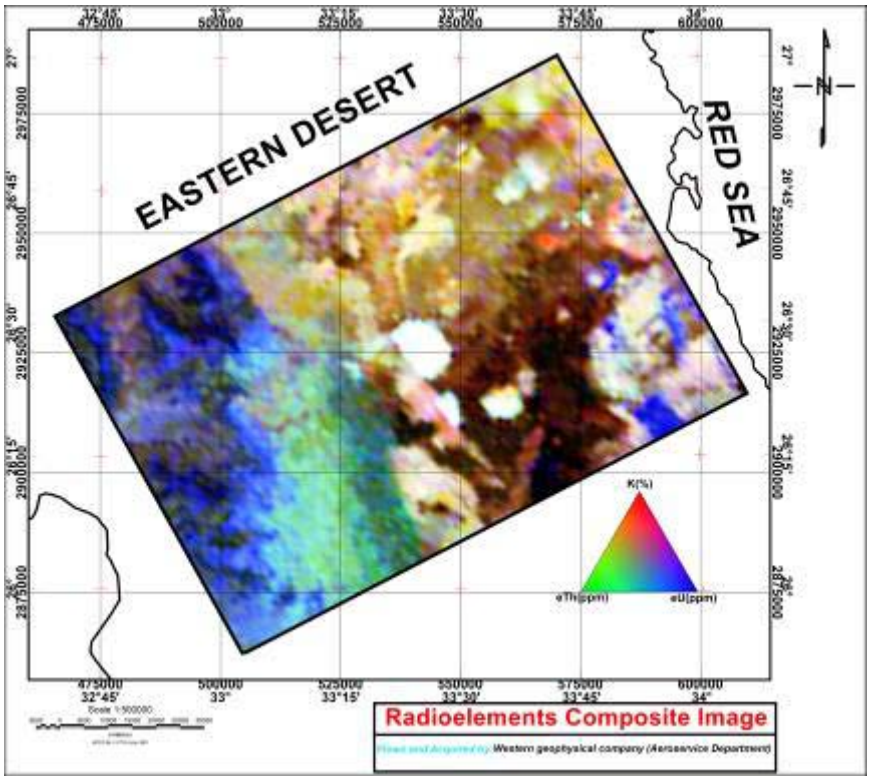

Figure (10): False Colour Radioelements Composite Image of Qena-Quseir Shear Zone area, Central Eastern Desert, Egypt.

b) Interpreted Radiometric Lithologic Unit (IRLU) Map

The construction of interpreted radiometric lithologic unit map can be achieved by applying the normality test and calculating the Chi-Square ($\chi 2$) test depending on total count values. The chi-square ($\chi 2$) test is carried out to test the degree of goodness of fit between the normal (theoretical) curve and the observed one. This test is used to measure the normality of the distribution by applying the following formula:

$$\chi^2 = \sum_{i=1}^{i=k} (f_i - F_i)^2 \Big/ F_i$$

where:

χ^2 = chi-square value,

k = total number of class intervals,

f_i = actual number of observations in the i^{th} category, and

F_i=theoretical frequency in the i^{th} category.

The area is covered by thirty three rock units of sedimentary rocks and basement complex, as given in the geologic map (Fig. 2). The univariate statistical analysis was carried out to obtain the arithmetic mean (X) and standard deviation (S) for each individual rock unit. The chi-square ($\chi 2$) test is applied to check the distribution of the variables, whether it is normal or non-normal. This was done by comparing the observed frequencies of the distribution with the theoretical normal curve having the same mean, standard deviation and total number of samples. After application of normality and chi square tests for every unit spectrometric data, it is found that there are twenty five rock units have normal histograms and eight don't have. The histograms of normal and non-normal rock units are represented in figures (11) and (12) respectively. The results of Chi-Square Test is tabulated in table (1). The rock units which is found to obey non-normal distribution are divided into two subunits as follow:

1- Melanocratic metamorphic rocks is divided statistically into two subunits, low total count subunit (gnm1) and high total count subunit (gnm2). The low total count subunit (gnm1) has a normal curve at category (k=7) and the high total count subunit (gnm2) has one at category number (k=8).
2- Metagabbro to metadiorite rocks is divided statistically into two subunits, low total count subunit (mg1) and high total count subunit (mg2). The low total count subunit (mg1) has a normal curve at category (k=11) and the high total count subunit (mg2) has one at category number (k=9).
3- Ohiolitic Metagabbro rocks is divided statistically into two subunits, low total count subunit (mgo1) and high total count subunit (mgo2). The low total count subunit (mgo1) has a normal curve at category (k=12) and the high total count subunit (mgo2) has one at category number (k=10).
4- Gabbroic rocks is divided statistically into two subunits, low total count subunit (gb1) and high total count subunit (gb2). The low total count

subunit (gb1) has a normal curve at category (k=10) and the high total count subunit (gb2) has one at category number (k=8).

5- Younger granite rocks is divided statistically into two subunits, low total count subunit (gβ1) and high total count subunit (gβ2). The low total count subunit ($g_{\beta}1$) has a normal curve at category (k=15) and the high total count subunit ($g_{\beta}2$) has one at category number (k=11).
6- Dakhla Formation is divided statistically into two subunits, low total count subunit (Kud1) and high total count subunit (Kud2). The low total count subunit (Kud1) has a normal curve at category (k=12) and the high total count subunit (Kud2) has one at category number (k=10).
7- Esna Formation is divided statistically into two subunits, low total count subunit (Tpe1) and high total count subunit (Tpe2). The low total count subunit (Tpe1) has a normal curve at category (k=10) and the high total count subunit (Tpe2) has one at category number (k=7).
8- Fanglomerate is divided statistically into two subunits, low total count subunit (Qf1) and high total count subunit (Qf2). The low total count subunit (Qf1) has a normal curve at category (k=11) and the high total count subunit (Qf2) has one at category number (k=11).

After the calculating of Chi-Square values of the non-normal rock units and dividing theses rock units into two subunits according to total count concentration, another Chi-Square test is also performed to the subunits to check if it obey normal or non-normal distribution. The results of the Chi-Square test of these subunits (Table 2) showed that these subunits are following normal distribution. Therefore, the normal units and normal subunits was used to construct the interpreted radiometric lithologic unit (IRLU) map (Fig. 13).

c) Location of Uraniferous Leads

The main target of aerial prospection using gamma ray spectrometric survey data is the delineation of expected boundaries of potential uraniferous areas, in which the varying rock units are enriched in uranium (Saunders & Potts 1976). The most important parameters, which can be measured, are relative concentrations of uranium to thorium and uranium to potassium, taken in conjunction with uranium measurements.

In this study, significant locations of eU anomalies are defined on the basis of calculation of probabilities, where their data differ significantly from the mean background, as defined by the data themselves, and at certain levels of probabilities these differences were computed. The high anomalous values are considered as the values equalling or exceeding at least two standard deviations from the calculated arithmetic mean values (X+2S) for eU, eU/eTh and eU/K measurements, for a single point in each rock unit. This acceptable technique was chosen for distinguishing between the normal and abnormal measurements, which could be anomalous values according to Saunders & Potts (1978) technique for calculating the significant factor of each radio-spectrometric variable in each rock unit. Calculations of arithmetic mean (X), standard deviation (S) and the values of (X+2S) for eU, eU/eTh and eU/K of each rock unit are summarized in tables (3, 4 & 5). Figure (14) shows the interpreted uranium point anomaly map of the study area, which possesses values exceeding X+2S for eU, eU/K and eU/eTh variables. Fifteen groups of statistically significant (anomalous) points can be distinguished on this map (Fig. 14). Anomalous locations are summarized in Table (6). The majority of uranium anomalous zones are related to younger granite, Duwi formation and parts of Dokhan volcanics.

V. Concolusion

Qualitative Interpretation of all radiospectrometric maps prove that the highest values are related to younger granite, Duwi formation and parts of Dokhan volcanics.

After application of normality and chi square tests for every unit spectrometric data, it is found that there are twenty five rock units have normal histograms and eight don't have. The rock units which is found to obey non-normal distribution are divided into two subunits. Another Chi-Square test is also performed to the subunits to check if it obey normal or non-normal distribution. The results of the Chi-Square test of these subunits showed that these subunits are following normal distribution. Therefore, the normal units and normal subunits was used to construct the interpreted radiometric lithologic unit (IRLU) map.

Significant locations of eU anomalies are defined on the basis of calculation of probabilities, where their data differ significantly from the mean background, as defined by the data themselves, and at certain levels of probabilities these differences were computed. Fifteen groups of statistically significant (anomalous) points can be distinguished on IRLU map. The majority of uranium anomalous zones are related to younger granite, Duwi formation and parts of Dokhan volcanics.

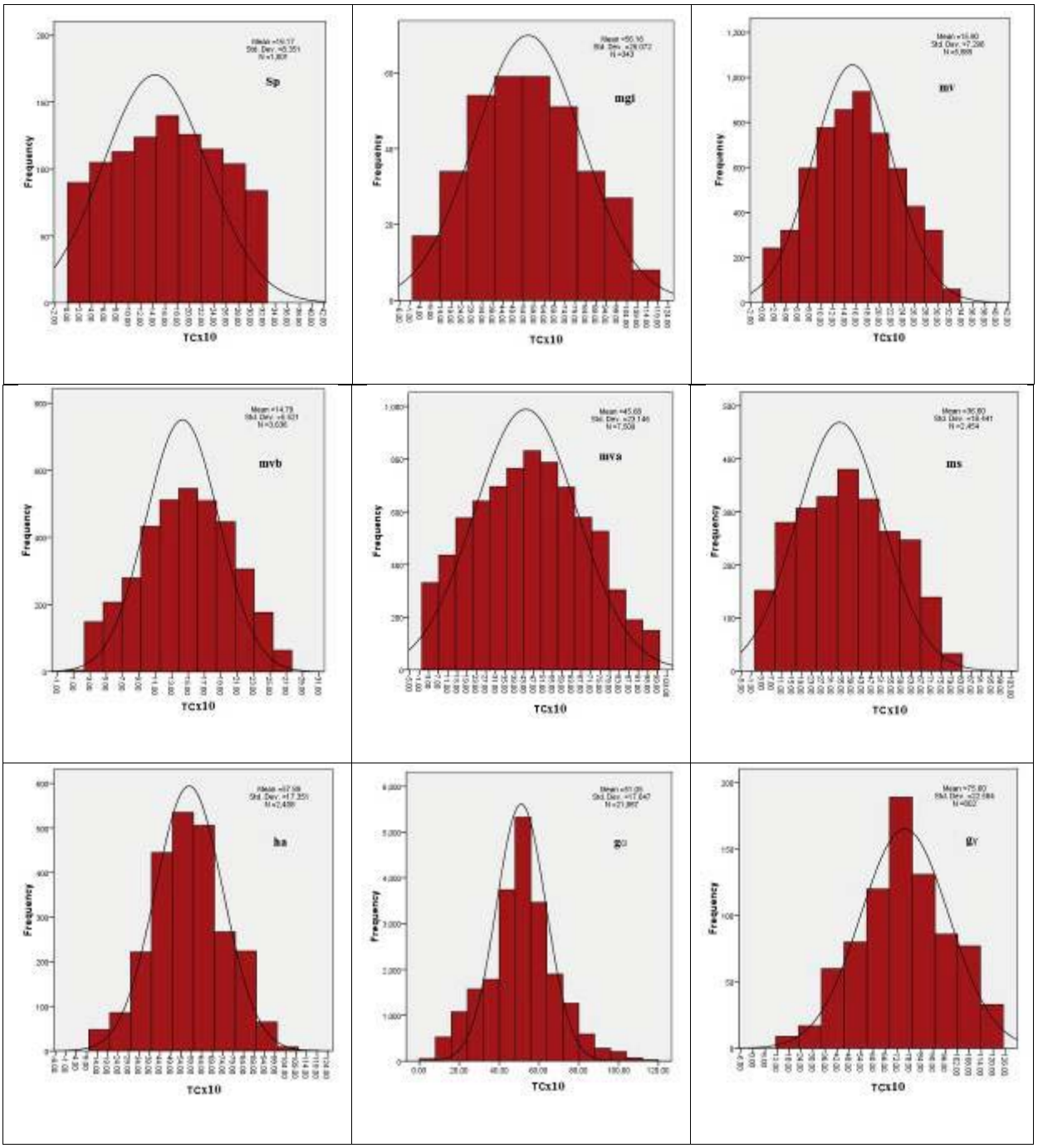

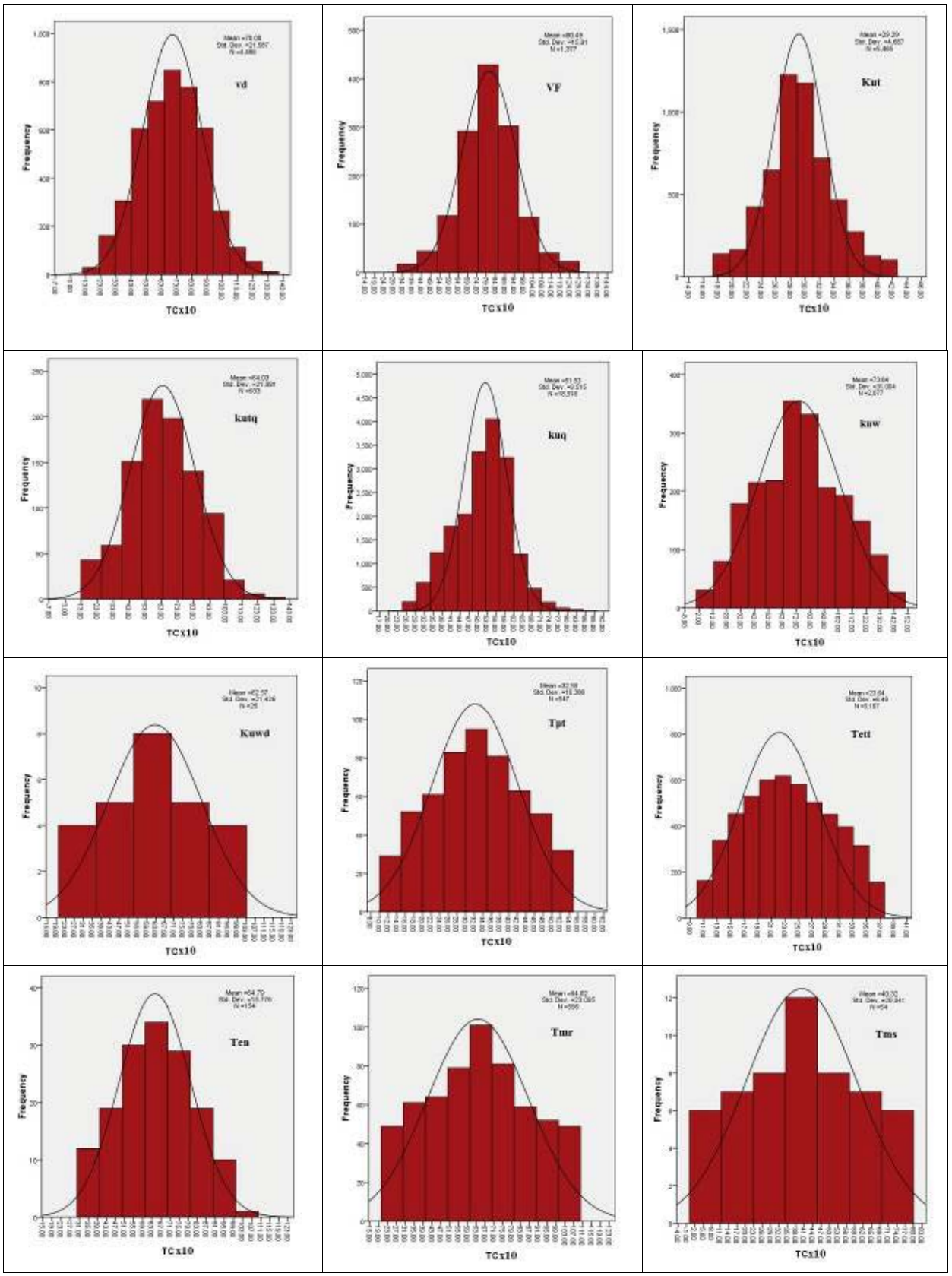

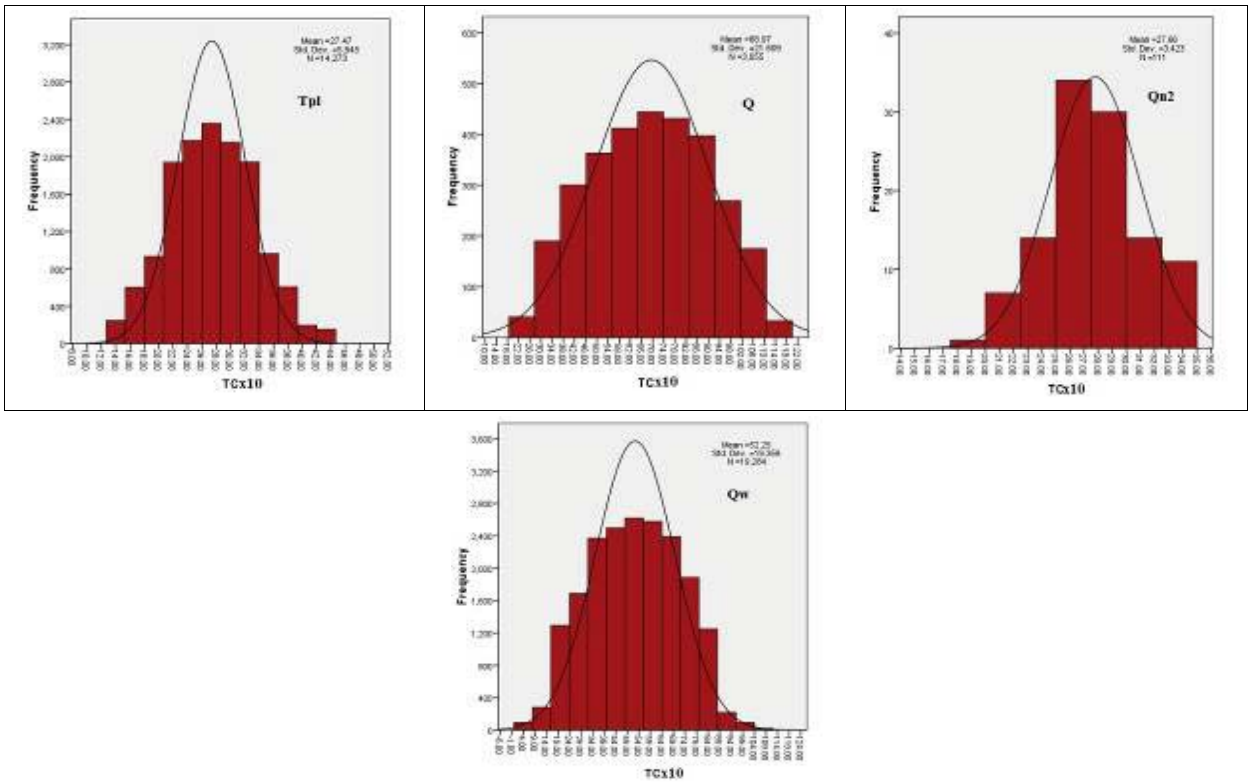

Figure (11): Frequency Distribution Histograms of Aerial Total Count Concentrations with Their Fitted Theoretical Curves of Normal Rock Units

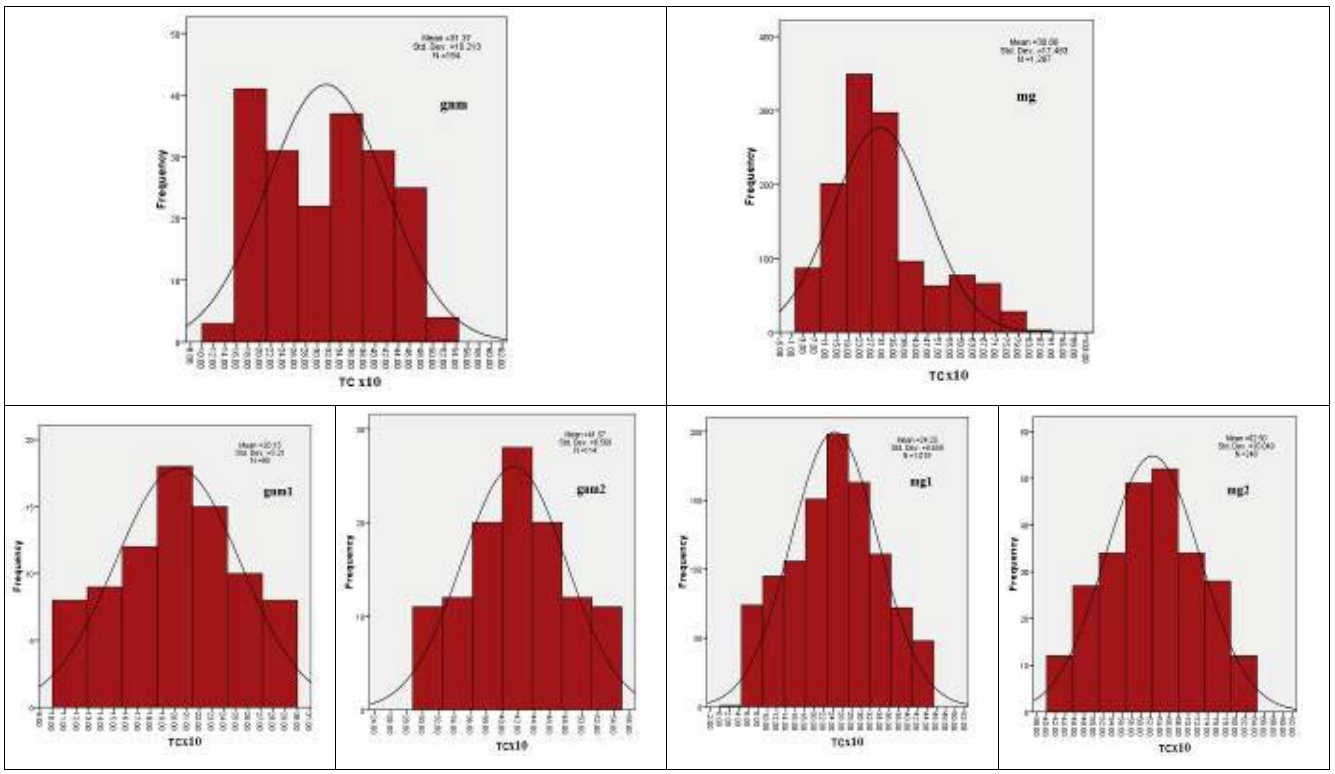

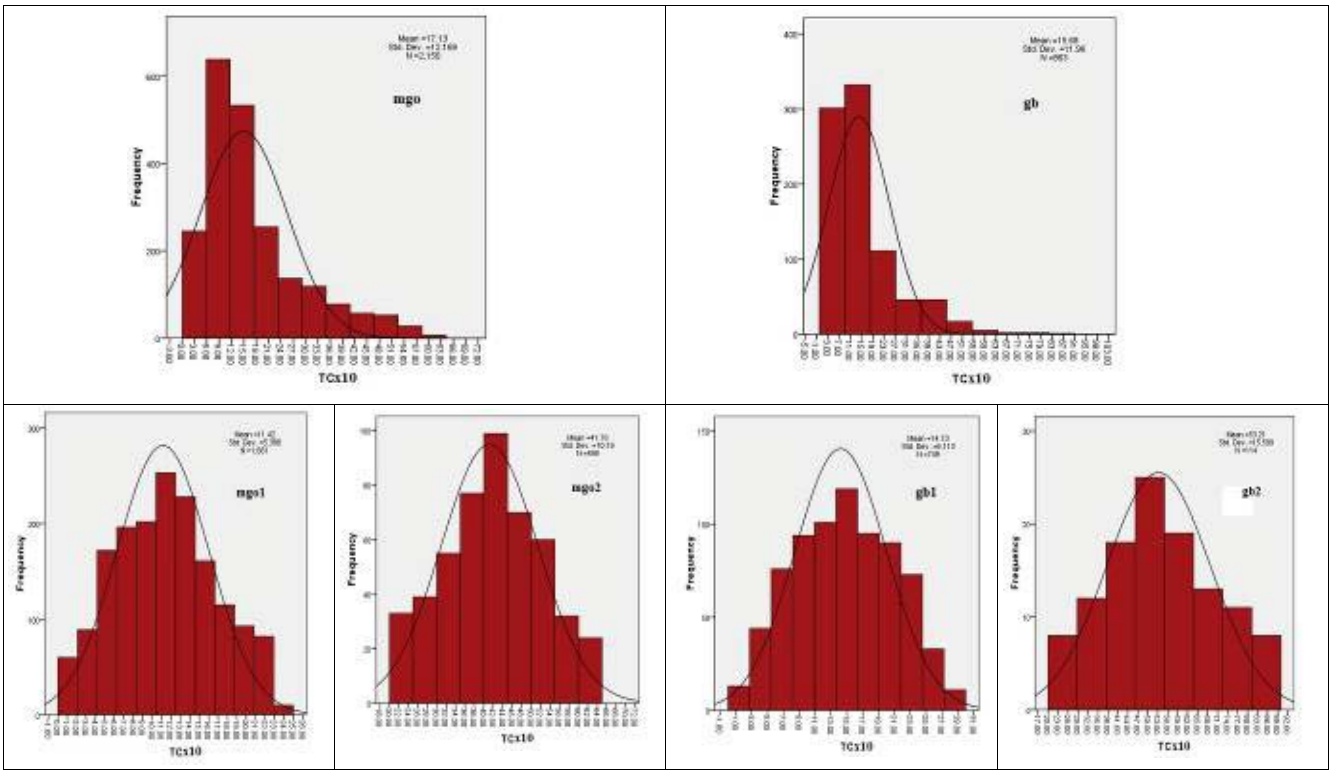

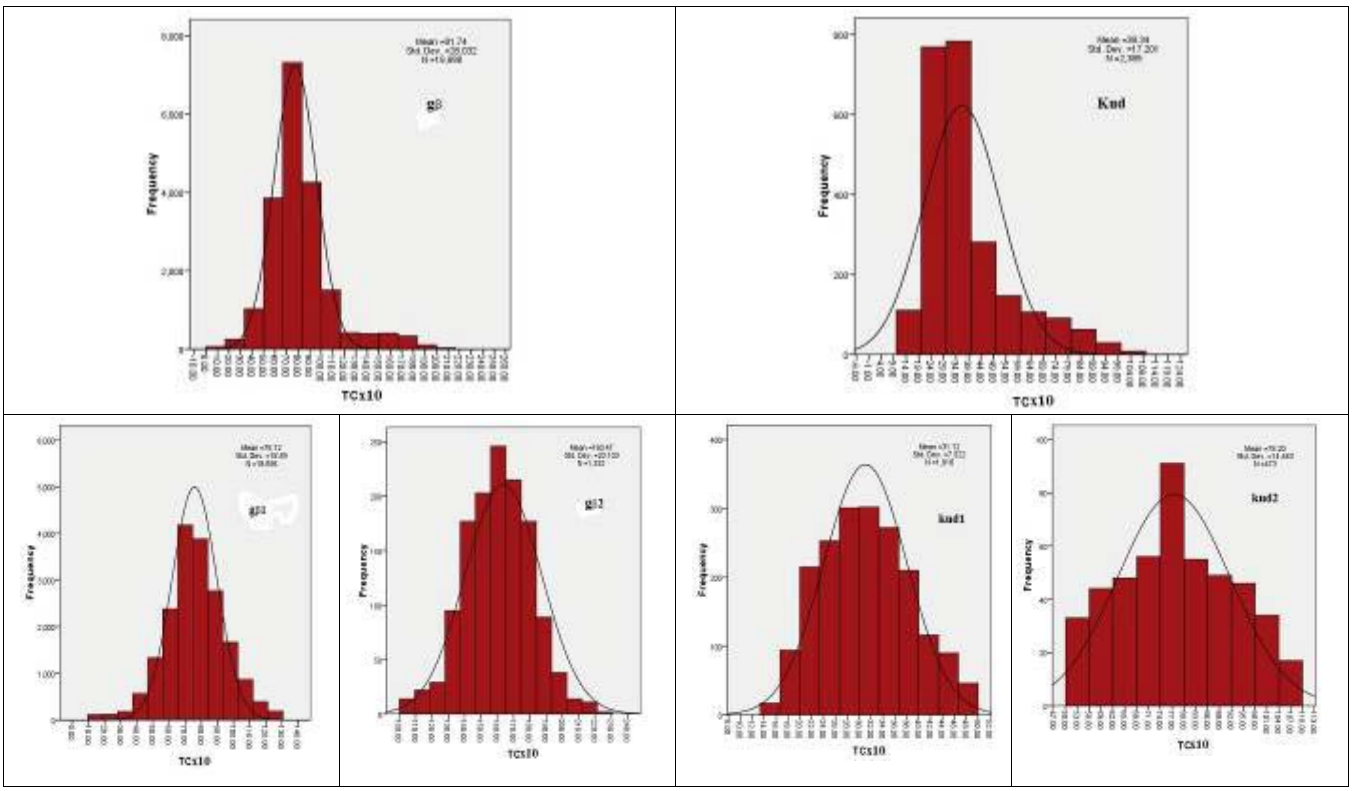

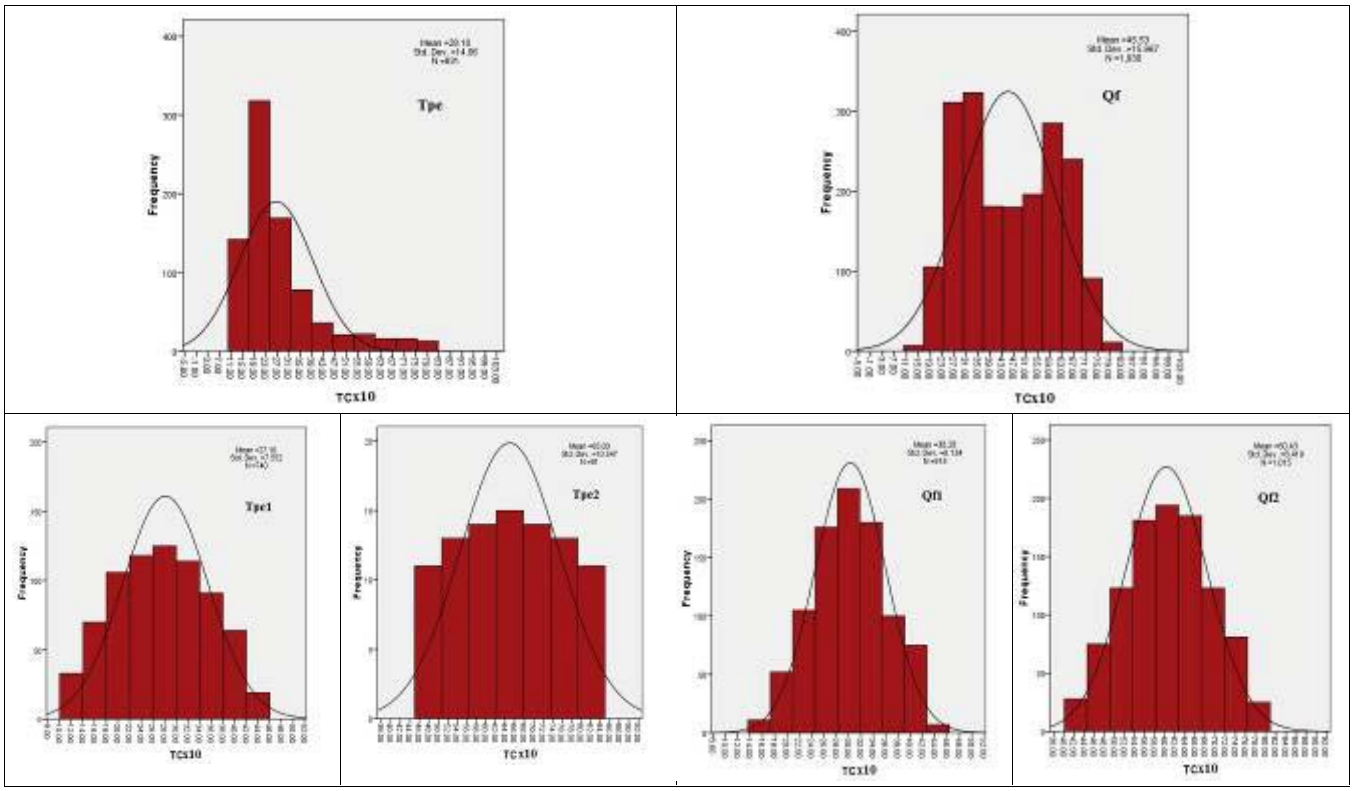

Figure (12): Frequency Distribution Histograms of Aerial Total Count Concentrations with Their Fitted Theoretical Curves of Non-Normal Rock Units and Its Subunits

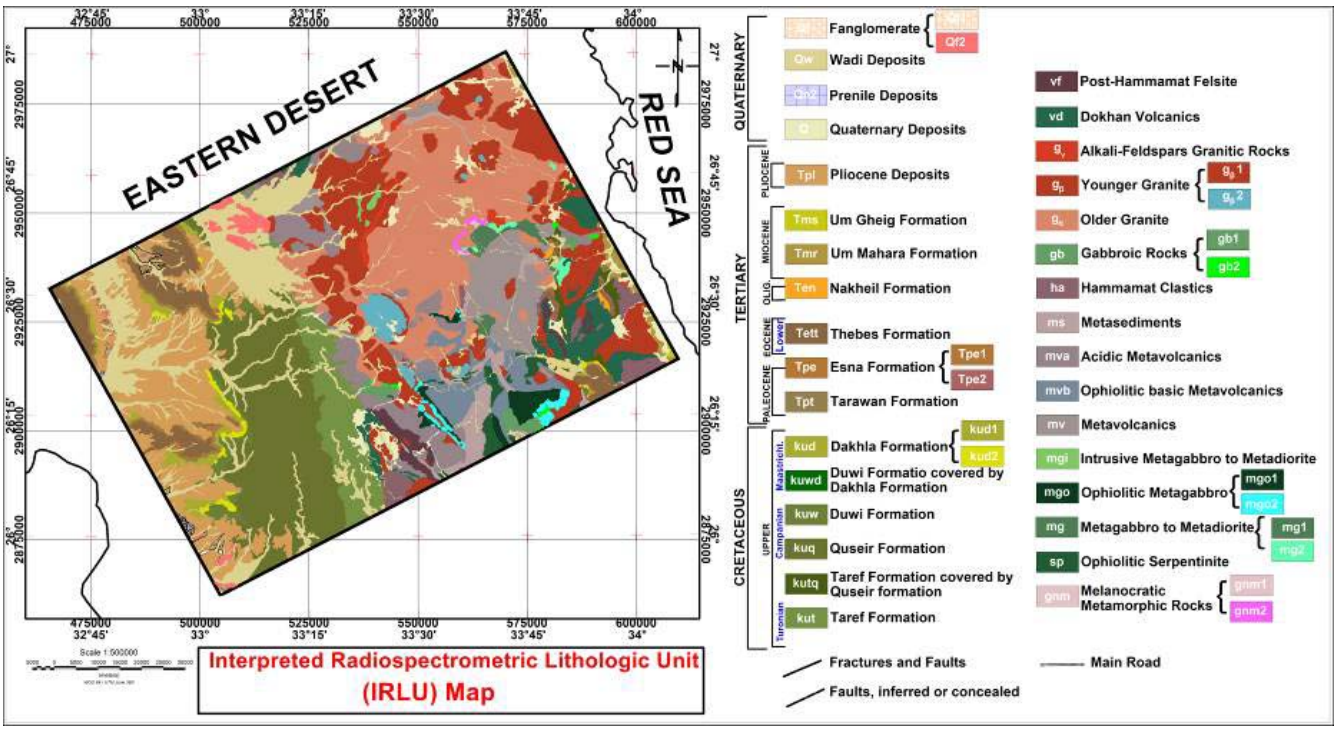

Figure (13): Interpreted Spectral Radiometric Lithological Unit (IRLU) Map of Qena-Quseir Shear Zone area, Central Eastern Desert, Egypt

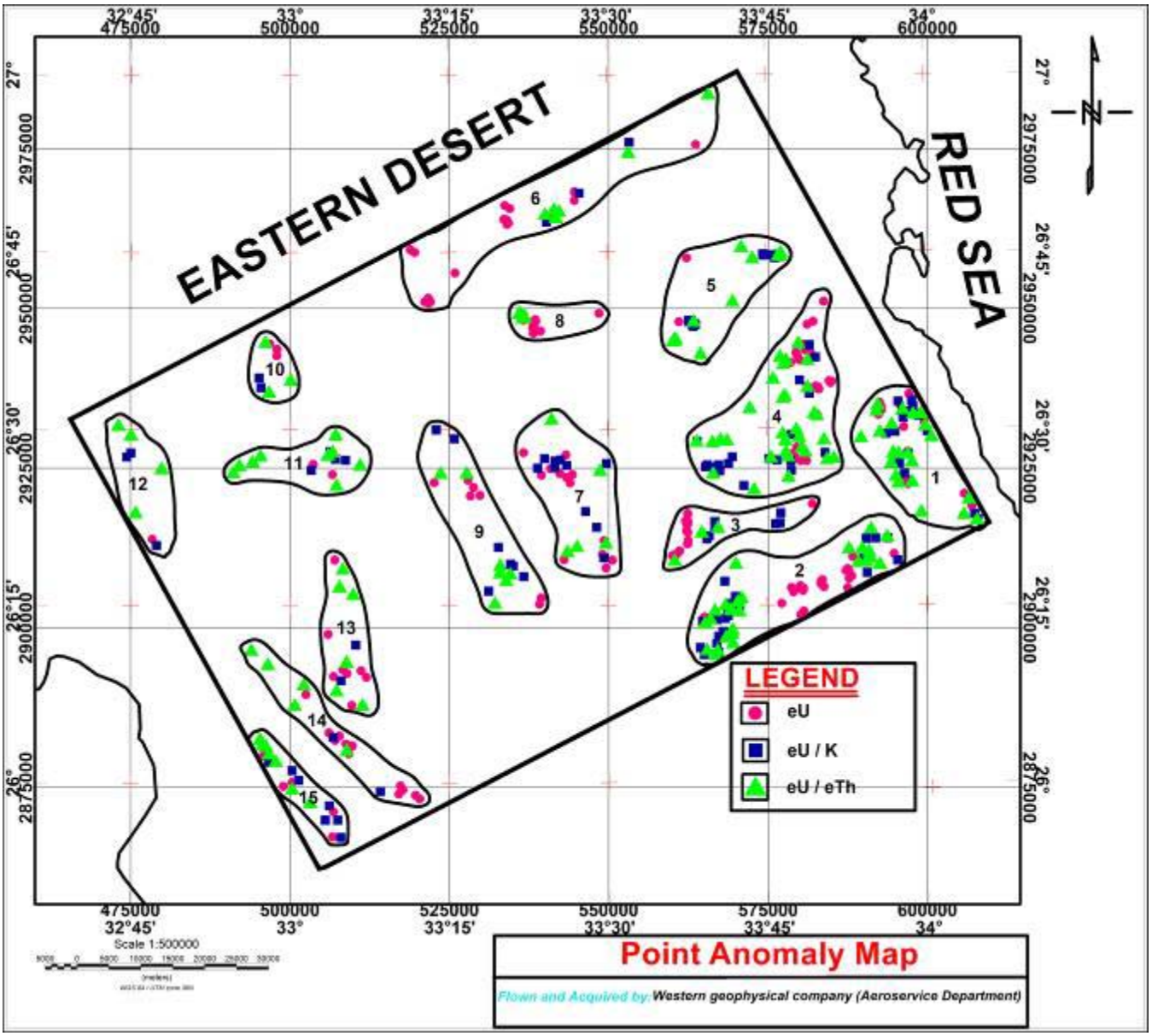

Figure (14): Uranium Point Anomaly Map of Qena-Quseir Shear Zone Area, Central Eastern Desert, Egypt

Table (1): Summary of the results of χ^2-test of the TC measurements of All Rock Units of Qena-Quseir Shear Zone Area, Central Eastern Desert, Egypt

No.	Rock Units	Theoritical Chi Value	Calculated Chi Value	K	Normality
1	gα	24.68	23.952	15	Normal
2	gβ	24.68	27.64	15	Not Normal
3	gb	19.68	22.01	11	Not Normal
4	gγ	19.68	18.67	11	Normal
5	gnm	16.92	19.51	9	Not Normal
6	ha	21.03	21.61	12	Normal
7	Kud	21.03	23.94	12	Not Normal
8	Kuq	24.68	28.76	15	Normal

9	Kut	22.36	21.98	13	Normal
10	Kutq	19.68	19.52	11	Normal
11	Kuw	21.03	21.5	12	Normal
12	Kuwd	12.22	12.08	6	Normal
13	mg	19.68	22.98	11	Not Normal
14	mgi	16.92	15.99	9	Normal
15	mgo	21.03	24.21	12	Not Normal
16	ms	21.03	21.52	12	Normal
17	mv	22.36	22.03	13	Normal
18	mva	23.68	24	14	Normal
19	mvb	22.36	22.05	13	Normal
20	Q	22.36	22.52	13	Normal
21	Qf	21.03	24.55	12	Not Normal
22	Qn2	15.05	14.74	8	Normal
23	Qw	24.68	24.59	15	Normal
24	Sp	19.68	19.23	11	Normal
25	Ten	15.05	14.52	8	Normal
26	Tett	22.36	22.05	13	Normal
27	Tmr	20.48	20.05	10	Normal
28	Tms	13.23	13.08	7	Normal
29	Tpe	19.68	24.06	11	Not Normal
30	Tpl	24.68	24.72	15	Normal
31	Tpt	20.48	20.91	10	Normal
32	Vd	22.36	22.52	13	Normal
33	Vf	19.68	19.73	11	Normal

Table (2): Summary of the results of χ^2-test of the TC measurements of Non-Normal Rock Units and Its Subunits of Qena-Quseir Shear Zone Area, Central Eastern Desert, Egypt

No.	Rock Units	SubUnits	Theoritical Chi	Calculated Chi	K	Normality
1	gnm	gnm1	13.23	13.12	7	Normal
		gnm2	15.05	14.81	8	Normal
2	mg	mg1	19.68	19.47	11	Normal
		mg2	16.92	16.78	9	Normal
3	mgo	mgo1	21.03	20.94	12	Normal
		mgo2	20.48	20.31	10	Normal
4	gb	gb1	20.48	20.27	10	Normal
		gb2	15.05	14.89	8	Normal
5	gβ	gβ1	24.68	24.09	15	Normal
		gβ2	19.68	19.51	11	Normal
6	Kud	Kud1	21.03	20.87	12	Normal
		Kud2	20.48	20.36	10	Normal
7	Tpe	Tpe1	20.48	20.25	10	Normal
		Tpe2	13.23	13.15	7	Normal
8	Qf	Qf1	19.68	19.55	11	Normal
		Qf2	19.68	19.43	11	Normal

Table (3): Statistical Analysis of the (eU) Content in the Different Lithologic Units

Data	L.U	Range		Mean(X)	S.D (S)	X+1S	X+2S	X+3S
		Mini.	Maxi.					
eU (ppm)	gnm	0.09	2.56	1.08	0.44	1.52	1.96	2.4
	sp	0	7.03	0.75	0.91	1.66	2.57	3.48
	mg	0.04	3.6	1	0.67	1.67	2.34	3.01
	mgo	0	4.03	0.77	0.58	1.35	1.93	2.51
	mgi	0.2	3.33	1.33	0.78	2.11	2.89	3.67
	mv	0	5.29	0.77	0.56	1.33	1.89	2.45
	mvb	0	6.78	0.64	0.49	1.13	1.62	2.11
	mva	0	7.88	1.45	0.96	2.41	3.37	4.33
	ms	0	6.11	1.15	0.78	1.93	2.71	3.49
	ha	0.18	12.24	2.38	0.99	3.37	4.36	5.35
	gb	0.04	2.07	0.68	0.43	1.11	1.54	1.97
	gα	0	16.02	1.66	0.92	2.58	3.5	4.42
	gβ	0	18.83	3.03	2.09	5.12	7.21	9.3
	gγ	0	4.92	2.23	0.96	3.19	4.15	5.11
	vd	0.27	8.54	2.75	0.99	3.74	4.73	5.72
	vf	0.78	8.17	2.93	0.98	3.91	4.89	5.87
	kut	0.53	4.91	1.97	0.48	2.45	2.93	3.41
	kutq	0.33	19.07	6.21	3.64	9.85	13.49	17.13
	kuq	0.76	18.15	3.19	1.53	4.72	6.25	7.78
	kuw	1.44	25.98	9.02	4.45	13.47	17.92	22.37
	kuwd	1.22	9.93	5.46	2.68	8.14	10.82	13.5
	kud	0.96	20.91	4.34	2.97	7.31	10.28	13.25
	Tpt	0.82	7.11	2.56	1.14	3.7	4.84	5.98
	Tpe	0.28	17.01	3.01	2.11	5.12	7.23	9.34
	Tett	0.74	12.94	2.13	1.22	3.35	4.57	5.79
	Ten	1.99	5.76	3.39	0.92	4.31	5.23	6.15
	Tmr	0.42	13	3.67	2.06	5.73	7.79	9.85
	Tms	0.13	3.72	1.52	1	2.52	3.52	4.52
	Tpl	0.44	17.4	2.42	1.3	3.72	5.02	6.32
	Q	0.14	13.32	3.09	1.64	4.73	6.37	8.01
	Qn2	1.75	2.66	2.11	0.17	2.28	2.45	2.62
	Qw	0	16.1	2.4	1.35	3.75	5.1	6.45
	Qf	0.84	5.8	2.42	0.72	3.14	3.86	4.58

Table (4): Statistical Analysis of the (eU / eTh) Content in the Different Lithologic Units

Data	L.U	Range		Mean(X)	S.D (S)	X+1S	X+2S	X+3S
		Mini.	Maxi.					
	gnm	0.05	0.56	0.35	0.1	0.45	0.55	0.65
	sp	0	5.05	0.68	0.55	1.23	1.78	2.33
	mg	0.02	1.43	0.35	0.14	0.49	0.63	0.77
	mgo	0	4.08	0.48	0.42	0.9	1.32	1.74
	mgi	0.06	0.62	0.27	0.11	0.38	0.49	0.6
	mv	0	7.56	0.4	0.27	0.67	0.94	1.21
	mvb	0	12.28	0.46	0.41	0.87	1.28	1.69
	mva	0	36.8	0.38	0.44	0.82	1.26	1.7
	ms	0	4.57	0.49	0.36	0.85	1.21	1.57

eU / eTh	ha	0.1	3.77	0.44	0.26	0.7	0.96	1.22
	gb	0.03	2.93	0.47	0.28	0.75	1.03	1.31
	gα	0	2.08	0.34	0.12	0.46	0.58	0.7
	gβ	0	3.27	0.37	0.12	0.49	0.61	0.73
	gγ	0	1.13	0.31	0.12	0.43	0.55	0.67
	vd	0.12	2.75	0.43	0.14	0.57	0.71	0.85
	vf	0.16	0.88	0.38	0.09	0.47	0.56	0.65
	kut	0.17	0.92	0.43	0.09	0.52	0.61	0.7
	kutq	0.23	6.86	1.63	1.31	2.94	4.25	5.56
	kuq	0.14	4.4	0.49	0.34	0.83	1.17	1.51
	kuw	0.31	6.88	2.13	1.05	3.18	4.23	5.28
	kuwd	0.39	2.13	1.04	0.52	1.56	2.08	2.6
	kud	0.27	6.21	1.46	0.81	2.27	3.08	3.89
	Tpt	0.32	4.13	1.2	0.51	1.71	2.22	2.73
	Tpe	0.16	6.02	1.39	0.77	2.16	2.93	3.7
	Tett	0.27	6.51	1.3	0.78	2.08	2.86	3.64
	Ten	0.32	3.25	0.78	0.57	1.35	1.92	2.49
	Tmr	0.06	6.03	0.95	0.87	1.82	2.69	3.56
	Tms	0.13	0.78	0.48	0.13	0.61	0.74	0.87
	Tpl	0.12	4.16	0.8	0.36	1.16	1.52	1.88
	Q	0.02	3.7	0.48	0.32	0.8	1.12	1.44
	Qn2	0.53	0.89	0.67	0.08	0.75	0.83	0.91
	Qw	0	4.96	0.54	0.36	0.9	1.26	1.62
	Qf	0.16	1.98	0.58	0.29	0.87	1.16	1.45

Table (5): Statistical Analysis of the (eU / K) Content in the Different Lithologic Units

Data	L.U	Range		Mean(X)	S.D (S)	X+1S	X+2S	X+3S
		Mini.	Maxi.					
eU / K	gnm	0.22	2.14	1.19	0.38	1.57	1.95	2.33
	sp	0	19.12	3.43	3.08	6.51	9.59	12.67
	mg	0.06	5.94	1.16	0.63	1.79	2.42	3.05
	mgo	0	20.15	1.9	2.07	3.97	6.04	8.11
	mgi	0.15	1.81	0.79	0.35	1.14	1.49	1.84
	mv	0	10.98	1.38	0.92	2.3	3.22	4.14
	mvb	0	16.83	1.78	1.41	3.19	4.6	6.01
	mva	0	8.85	1.35	0.78	2.13	2.91	3.69
	ms	0	37.2	1.59	1.52	3.11	4.63	6.15
	ha	0.28	22.11	1.64	1.43	3.07	4.5	5.93
	gb	0.06	11.61	2.12	1.55	3.67	5.22	6.77
	gα	0	13.37	1.04	0.47	1.51	1.98	2.45
	gβ	0	6.64	1.22	0.67	1.89	2.56	3.23
	gγ	0	3.91	0.86	0.43	1.29	1.72	2.15
	vd	0.47	18.55	1.44	0.7	2.14	2.84	3.54
	vf	0.49	3.12	1.19	0.35	1.54	1.89	2.24
	kut	0.48	49.97	4.62	2.12	6.74	8.86	10.98
	kutq	0.73	52.82	9.83	10.11	19.94	30.05	40.16
	kuq	0.52	36.97	4.43	3.28	7.71	10.99	14.27
	kuw	1.53	58.75	18.07	9.2	27.27	36.47	45.67

	kuwd	1.27	7.51	3.45	1.66	5.11	6.77	8.43
	kud	1.53	58.75	12.2	7.32	19.52	26.84	34.16
	Tpt	2.02	40.62	9.41	5.58	14.99	20.57	26.15
	Tpe	0.3	36.81	9.73	5.97	15.7	21.67	27.64
	Tett	1.22	47.09	8.79	5.87	14.66	20.53	26.4
	Ten	1.12	24.03	3.45	3.98	7.43	11.41	15.39
	Tmr	0.16	33.82	3.94	4.88	8.82	13.7	18.58
	Tms	1.03	2.66	1.69	0.45	2.14	2.59	3.04
	Tpl	0.55	47.44	5.89	3.55	9.44	12.99	16.54
	Q	0.06	18.99	1.86	1.65	3.51	5.16	6.81
	Qn2	3.51	7.18	4.92	0.79	5.71	6.5	7.29
	Qw	0	33.12	3.03	3.34	6.37	9.71	13.05
	Qf	0.67	24.55	3.4	2.75	6.15	8.9	11.65

Table (6): Anomalous Locations at Qena-Quseir Shear Zone Area, Central Eastern Desert, Egypt

No	UTM of anomaly Center		Trend	Anomaly Result From	Rock Types	Rocks Location
	X	Y				
1	598414	2925427	NW-SE	eU, eU/K, eU/eTh	gβ-Vd-ha-Kuwd-Kutq-Tmr-Tett-Q	East G. Umm Zarabit
2	579925	2906524	ENE-WSW	eU, eU/K, eU/eTh	gβ-Vd-ha-Kuw-Kutq-mgo-gb-ms	South G. Halham
3	570405	2916596	ENE-WSW	eU, eU/K, eU/eTh	gβ-Vd-mv-mvb-gb-ms-sp	NE G. Umm El-Abas
4	576338	2933567	NE-SW	eU, eU/K, eU/eTh	gβ-gα-Vd-mg-ms-mv-Vf-Tett-Tpt	NE G. Abu-Aqarib
5	566128	2953436	ENE-WSW	eU, eU/K, eU/eTh	gβ-gα-mgi-mg-gnm-Q	NW G. Nuqara
6	539843	2967164	ENE-WSW	eU, eU/K, eU/eTh	gβ-gα-mv-mva-Vd-ha-ms-Q	G. Fatira
7	545362	2919977	N-S	eU, eU/K, eU/eTh	gβ-gα-ms-mvb-mva-gb	West G. Semna
8	542051	2947572	E-W	eU, eU/eTh	gβ-gα-mgi-Q-Kut-Kuq	G. Abu-Shihat
9	529357	2915286	NNW-SSE	eU, eU/K, eU/eTh	gα-mva-Vd-Q	West G. Missikat El-Gukh
10	497623	2940121	N-S	eU, eU/K, eU/eTh	Tpl-Qw-Kud-Tett-Ten-Tmr	G. Abu-Had
11	501762	2925496	E-W	eU, eU/K, eU/eTh	Tpl-Kuw-Kud-Tett-Ten-Tmr-Kuq	North G. Qreiya
12	476375	2922460	N-S	eU/K, eU/eTh	Tpl-Tpt-Tpe-Ten-Tmr-Kud-Qf-Qn2	NW W. El-Qreiya
13	508661	2898177	N-S	eU, eU/K, eU/eTh	Kuw-Kuq-Kud-Qw-Ten-Tmr	West W. El-Atwani
14	507557	2882724	NW-SE	eU, eU/K, eU/eTh	Tpl-Tpe-Ten-Tett-Kuw-Kud-Kuq	West W. Abu-Tenadib
15	502038	2874169	NW-SE	eU, eU/K, eU/eTh	Qw-Qf-Qn2-Tpl-Kuw	West W. Abu-Tenadib

References Références Referencias

1. Aero-Service, 1984: Final operational report of airborne magnetic/radiation survey in the Eastern Desert, Egypt For the Egyptian General Petroleum Corporation (EGPC) and the Egyptian Geological Survey and Mining Authority (EGSMA), Aero-Service Division, Houston, Texas, USA, Six Volumes.
2. Conco Coral and EGPC, 1987: Geological map of Egypt, scale 1: 500,000
3. Duval, J. S., 1983: Composite colour images of aerial gamma -ray spectrometric data. Geophysics, Vol. 48 No.16, pp. 722-735.
4. El-Gaby, S., 1983: Architecture of the Egyptian basement complex. Proceedings of the Fifth Intern. Conf. on Basement Tectonics, Cairo, Egypt.
5. El Ramly, M.F., 1972: A new geological map for the basement rocks in the Eastern and south Western Deserts of Egypt, (1:1,000,000). Ann. Geol. Surv. Egypt 11, 1–18.
6. Greiling, R. O., Kroner, A., El-Ramly, M. F. and Rashwan, A. A., 1988: Structural relationship between the southern and central Eastern Deserts of Egypt. Details of a fold and thrust belt. In. S. El-Gaby, and Greiling R.O., (Eds.). The Pan-African of

NE African and Adjacent Areas, Vieweg, Wieshaden, pp. 121 –145.

7. Habeib, M. S., Ahmed, A. A. and El-Nady, O. M., 1985: Two orogenies in the Meatiq area of Central Eastern Desert, Egypt. Precambrian Res., V. 30, pp. 83 - 111.
8. Ries, A. C., Shackleton, R. M., Graham, R. H. & Fitches, W. R., 1983: Pan-African structures, ophiolites and mélange in the Eastern Desert of Egypt: A traverse at 26° N. J. Geol. Soc., London, U K, V. 14, pp. 75 - 95.
9. Saunders, D. F. and Potts, M.J., 1976: Interpretation and application of high sensitivity airborne gamma ray spectrometric data. In: IAEA Symp. Exploration for Uranium Ore Deposits, Vienna, pp. 107-124.
10. Saunders, D.F., and Potts, M.J., 1978: Manual for application of NURE 1974–1977 aerial gamma-ray spectro-metric data: U.S. Department of Energy, Grand Junction office, Report GJBX–13(87), 183 p.
11. Schandelmeier H., Richter, A. and Franz, G., 1983: Outline of the geology of magmatic and metamorphic units from Gabal Uweinat to Bir Safsaf. Jour. Afr. Earth Sci., V. 1, pp. 275 - 283.
12. Schandelmeier, H., Daryshire, D. P. F., Harms U. and Richter, A., 1987: The east Sahara Craton-Evidence for Pre-PanAfrican crust in NE Africa, west of the River Nile. In. The Pan-African Belt of NE Africa and Adjacent Area, El-Gaby and Greiling R. O. (eds.), Earth Evol. Sci., 1988, Andreas Vogel, Berlin, Germany.
13. Schurmann, F.W., 1974: Bemerkungen zur Funktion der Corpora pedunculata im Gehirn der Insekten aus morphologisher Sicht. Exp.Brain Res. 19, pp. 406–432.
14. Shackleton R. M., Ries, A. C., Graham, R. H. and Fitches, W. R., 1980: Late Precambrian ophiolitic mélange in the Eastern Desert of Egypt. Nature, V. 285, pp. 472 -274.
15. Sultan, M., Arvidson, R. E., Duncan, I. J., Stern, R. J. & EL Kaliouby, B. (1988): Extension of the Najd Shear System from Saudi Arabia to the Central Eastern Desert of Egypt based on integrated field and Landsat observations. - Tectonics, 7, pp. 1291-1306.